empirically that the F10.7 number correlates well with ionospheric conductivity[8].

The sunlit (hence summer) hemisphere measurements seem to show a relatively clear solar cycle variation, with a pronounced minimum in auroral frequency around the solar maximum (about 1990). Under conditions of darkness, no clear solar cycle trend exists, or at least none that is clear enough to extract from the available 12-year stretch of data. Because most intense aurorae occur in darkness (both because they are more frequent when the ionosphere is not sunlit[4] and because the local time of most intense aurorae (18:00 to 24:00 MLT) is in darkness for most of the year), the net effect is that solar cycle plays a relatively minor role in total precipitating energy-flux input into the ionosphere from intense aurorae. It will be helpful if the DMSP program continues for one or more additional solar cycles to help verify these results.

Although the yearly averages are of intrinsic interest, this approach is not the best for determining whether ionizing solar radiation is involved directly in suppressing the formation of intense aurorae. Over the course of a year both the frequency of aurorae and the F10.7 number can undergo substantial variations. It is therefore more useful to sort aurorae directly according to the 'instantaneous' (daily) value of F10.7 at the time of observation. The results of this approach are shown in Fig. 2. Each data point represents the time-averaged occurrence rate of aurora over the 12-year period 1984–1995 such that the daily F10.7 number was within the appropriate bin.

The F10.7 number determines the mean auroral frequency with a high degree of precision (correlation coefficient of −0.96) under sunlit conditions (Fig. 2a). Under dark conditions there is no correlation (−0.01) between the F10.7 number and auroral frequency (Fig. 2b). Taken together, these results are very powerful evidence that it is not some hidden variable indirectly related to solar cycle (such as solar-wind velocity or density) that produces the F10.7 effect but the presence of ionizing solar radiation itself. Indeed, we computed the hourly average values of various solar-wind parameters observed by the NASA IMP-8 satellite from 1984 to 1995; they scarcely varied. The high correlation coefficient under sunlit conditions does not mean that auroral frequency is uniquely determined by the F10.7 number (for example, in a large sample size, the mean height of children in a given age bin will be highly correlated with age, yet age alone does not determine an individual child's height).

No single theory for auroral arc formation has widespread acceptance[9], although the results are increasingly constraining. The electron acceleration process occurs between approximately 1–3 Earth radii above the surface of the Earth, and occurs in upward regions of field-aligned currents flowing between the ionosphere and the magnetosphere[10,11]. Most recently, it has been shown that intense aurorae, which occur most often in the 18:00–24:00 MLT sector, are three times less frequent when this sector is under sunlit conditions than in darkness[4]. These findings have previously led us to endorse the ionospheric feedback mechanism for auroral arc formation[12]. The dynamics of magnetospheric plasma, including magnetic substorms, require geomagnetic field-aligned currents driven from near-Earth space into, across and back out of the ionosphere. The ionospheric conductivity feedback hypothesis starts by noting that an unstable situations exists when insufficient conductivity exists in the ionosphere to support these imposed currents. The rapidly changing density gradients that exist above the ionosphere can make electromagnetic wave resonances possible. The resulting acceleration of electrons to keV energies creates sufficient ionospheric conductivity to complete the circuit. More-over, once a localized region of enhanced ionospheric conductivity is started, more current is directed towards that region, carried by additional precipitating electrons, which then further enhance the localized conductivity. The findings reported here strongly support the ionospheric conductivity feedback mechanism for auroral arc formation.   □

1. Schröder, W. *Das Phänomen des Polarlichts* (Wissenschaftliche Buchgesellschaft, Darmstadt, 1984).
2. Chamberlain, J. W. *The Physics of Aurora and Airglow* (American Geophysical Union, Washington DC, reprinted 1996).
3. Barth, C. A. in *The Upper Mesosphere and Lower Thermosphere: A Review of Experiment and Theory* (ed. R. M. Johnson, R. M. & Killeen, T. L.) 225–233 (American Geophysical Union, Washington DC, 1995).
4. Newell, P. T., Meng, C.-I. & Lyons, K. M. Suppression of discrete aurora by sunlight. *Nature* **381,** 766–767 (1996).
5. Newell, P. T., Lyons, K. M. & Meng, C.-I. A large survey of electron acceleration events. *J. Geophys. Res.* **101,** 2599–2614 (1996).
6. Hardy, D. A. *et al.* Report no. AFGL-TR-84-0317 (Air Force Geophysics Laboratory, Boston, MA, 1984).
7. Evans, D. S. The observations of a near monoenergetic flux of auroral electrons. *J. Geophys. Res.* **73,** 2315–2323 (1968).
8. Rasmussen, C. E., Schunk, R. W. & Wickwar, V. B. A photochemical equilibrium model for ionospheric conductivity. *J. Geophys. Res.* **93,** 9831–9840 (1988).
9. Borovsky, J. E. Auroral arc thicknesses as predicted by various theories. *J. Geophys. Res.* **98,** 6101–6138 (1993).
10. Lyons, L. R. Generation of large-scale regions of auroral currents, electric potentials, and precipitation by the divergence of the convection electric field. *J. Geophys. Res.* **85,** 17–24 (1980).
11. Block, L. P. & Fälthammar, C.-G. in *Auroral Physics* (eds Meng, C.-I., Rycroft, M. J. & Frank, L. A.) 109–118 (Cambridge Univ. Press, 1991).
12. Lysak, R. J. Feedback instability of the ionospheric resonant cavity. *J. Geophys. Res.* **96,** 1553–1568 (1991).

Implementation of a quantum search algorithm on a quantum computer

Jonathan A. Jones[*†], **Michele Mosca**[†‡] **& Rasmus H. Hansen**[†]

* Oxford Centre for Molecular Sciences, New Chemistry Laboratory, South Parks Road, Oxford OX1 3QT, UK
† Centre for Quantum Computation, Clarendon Laboratory, Parks Road, Oxford OX1 3PU, UK
‡ Mathematical Institute, 24–29 St Giles', Oxford OX1 3LB, UK

In 1982 Feynman[1] observed that quantum-mechanical systems have an information-processing capability much greater than that of corresponding classical systems, and could thus potentially be used to implement a new type of powerful computer. Three years later Deutsch[2] described a quantum-mechanical Turing machine, showing that quantum computers could indeed be constructed. Since then there has been extensive research in this field, but although the theory is fairly well understood, actually building a quantum computer has proved extremely difficult. Only two methods have been used to demonstrate quantum logic gates: ion traps[3,4] and nuclear magnetic resonance (NMR)[5,6]. NMR quantum computers have recently been used to solve a simple
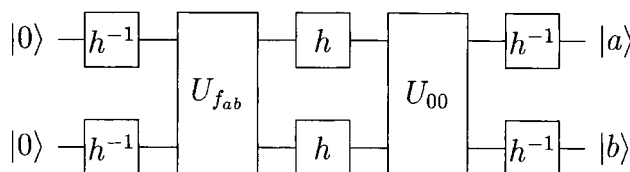

Figure 1 A quantum circuit for the implementation of a quantum search algorithm on a two-qubit computer. Gates marked h (pseudo-Hadamard gates) act to take a single eigenstate to a uniform superposition of the four possible eigenstates, whereas gates marked h^{-1} implement the inverse operation. The first two qubit gate $U_{f_{ab}}$ corresponds to an evaluation of the function f_{ab}, replacing an eigenstate $|ij\rangle$ by $-|ij\rangle$ if $i = a$ and $j = b$, whereas U_{00} simply replaces $|00\rangle$ by $-|00\rangle$.

quantum algorithm—the two-bit Deutsch problem[7,8]. Here we show experimentally that such a computer can be used to implement a non-trivial fast quantum search algorithm initially developed by Grover[9,10], which can be conducted faster than a comparable search on a classical computer.

Among other applications, Grover's algorithms enable an extremely rapid search over the domain of a binary function to find elements for which this function is satisfied (that is, the function has the value 1). This approach is simpler if the number of satisfying values is known beforehand, and is particularly simple when precisely one-quarter of the elements in the domain satisfy the function[11]. The algorithm can be demonstrated by using a computer with two quantum bits (qubits) to search a two-bit domain in which one of the four elements satisfies the function. A classical search of this domain would require between one and three evaluations of the function to find the satisfying element, whereas a quantum search can find this element with only one function evaluation. In the more general case of searching a domain of size N for one of k satisfying elements, the classical search requires about $\frac{1}{2}(N/k)$ function evaluations, whereas the quantum search[11] requires only $O(\sqrt{N/k})$.

A quantum circuit for implementing a quantum search in a two-qubit system is shown in Fig. 1. This algorithm uses a single function evaluation to label the single state that satisfies the function, followed by a series of gates that drive the system into this particular state. There are four possible functions f with a unique satisfying element, and these functions are conveniently labelled by the bit pattern of the satisfying element. The algorithm starts with the quantum computer in state $|00\rangle$ and ends with the computer in a state corresponding to the bit pattern of the unique element, and so this element can be immediately identified by determining the final state of each qubit.

This algorithm was implemented with our two-qubit NMR quantum computer, described in ref. 7. This computer uses the two spin states of ^{1}H nuclei in a magnetic field as qubits, and radio-frequency (RF) fields and spin–spin couplings between the nuclei are used to implement quantum logic gates. Our molecule, partially deuterated cytosine, contains two ^{1}H nuclei, and thus can be used to implement a two-qubit computer. The pseudo-Hadamard gates (h) were implemented by using 90°_y pulses; the function evaluation was performed with the pulse sequence shown in Fig. 2. The phases of five of the pulses depend on which of the four possible functions is to be implemented, and these phases should be set as shown in the figure caption. The final gate, U_{00}, is easily implemented, as it is identical to $U_{f_{00}}$.

The algorithm should start with the computer in state $|00\rangle$, but with an NMR quantum computer it is not practicable to begin in a true $|00\rangle$ state. By using the methods of Cory et al.[5] it is, however, possible to create an effective pure state, which behaves in an

equivalent manner. Similarly it is not practicable to determine the final state directly, but an equivalent measurement can be made by exciting the spin system with a further 90° pulse and observing the phases of the resulting NMR signals. The absolute phase of an NMR signal depends in a complex manner on a variety of experimental details, so it is not possible to interpret absolute phases, but this can be overcome by measuring a reference signal, obtained by applying a 90° pulse directly to the initial state.

The results of this approach are shown in Fig. 3. Five spectra are shown: a reference spectrum acquired by using a single 90° pulse, and spectra acquired from the same computer implementing the search algorithm for each of the four possible functions, f. Each spectrum consists of two closely spaced pairs of lines: each pair of lines corresponds to a single qubit, whereas the barely visible splitting within each pair arises from the spin–spin coupling, J, used to implement the two-qubit gates. To improve the appearance of the spectra the final 90° detection pulse was preceded by a magnetic field gradient pulse, which acts to dephase most of any error terms that might occur.

The reference spectrum corresponds to the computer's being in state $|00\rangle$, and the phase of this spectrum was adjusted so that both lines are in positive absorption phase (that is, pointing upwards). The same phase correction was then applied to the other four spectra, allowing positive absorption lines to be interpreted as qubits in state $|0\rangle$, whereas negative absorption lines can be interpreted as qubits in state $|1\rangle$. The left-hand pair of lines arises from the first spin, and thus corresponds to the first qubit; the right-hand pair of lines corresponds to the second qubit. Thus, for example, spectrum c in Fig. 3 corresponds to the state $|01\rangle$. Examining the four spectra b–e, it is clear that our implementation of a quantum search with the function f_{ab} leaves the computer largely in a final state $|ab\rangle$, much as expected.

There are, however, small but significant errors in the calculation, which result in distortions in the final spectra. Although most of these distortions are removed by the field gradient pulse, their effects remain visible as variations in the heights of the NMR lines. These errors arise from a variety of causes, but the most significant is errors in the NMR pulse sequence used to implement the calcula-
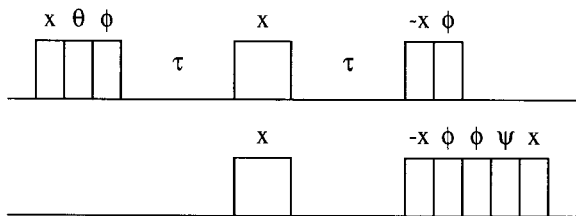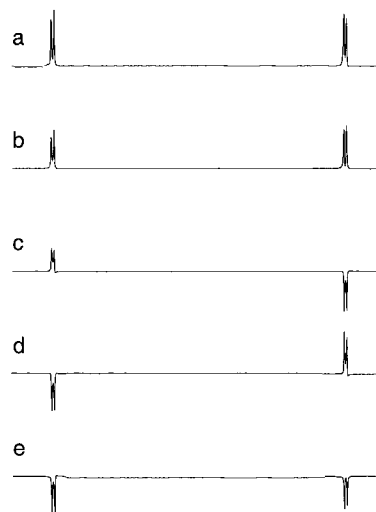

Figure 2 NMR pulse sequence used to implement $U_{f_{ab}}$. Narrow boxes correspond to 90° pulses, whereas wide boxes are 180° pulses; the upper and lower lines refer to the nuclear spins corresponding to the first and second qubits, respectively. The time period τ, during which no pulses are applied, is set equal to $1/4J$, where J is the size of the spin–spin coupling between the nuclei. The phase of each pulse is written above it, and for five of the pulses this phase depends on which of the four functions f_{ab} is to be implemented. These phases should be set as follows: f_{00}, $\theta = +y$, $\phi = +x$, $\psi = -y$; f_{01}, $\theta = +y$, $\phi = -x$, $\psi = +y$; f_{10}, $\theta = -y$, $\phi = -x$, $\psi = -y$; f_{11}, $\theta = -y$, $\phi = +x$, $\psi = +y$.

Figure 3 Experimental spectra from our NMR quantum computer. Spectrum a is a reference spectrum, used to determine the absolute phases of the NMR signals; spectra b–e were acquired from the same computer implementing the quantum search algorithm using each of the four possible functions: b, f_{00}; c, f_{01}; d, f_{10}; e, f_{11}. These four spectra were processed using the reference phase obtained from spectrum a, so the phases of the signals can be interpreted as states of the corresponding qubits, as described in the text.

tion. These pulse sequences require a large number of selective pulses, that is, pulses affecting only one of the two spins making up the computer. In practice it is difficult to achieve the desired effect at one spin while leaving the other entirely unaffected, resulting in errors in the final result. Interestingly the distortions are much worse in some cases than in others: they are particularly bad in the spectrum obtained when the function is f_{01}. Understanding this variability could lead to techniques for reducing the distortion in all cases.

Implementing Grover's algorithm is a major step forward for NMR quantum computing (since this Letter was first submitted, an implementation of Grover's algorithm by using heteronuclear NMR has been published[12]), but is by no means the limit of what can be achieved. Preliminary studies have been made of systems containing three qubits[13], and it should be possible to build larger NMR quantum computers, allowing the implementation of more complex algorithms. □

1. Feynman, R. P. Simulating physics with computers. *Int. J. Theor. Phys.* **21,** 467–488 (1982).
2. Deutsch, D. Quantum-theory, the Church–Turing principle and the universal quantum computer. *Proc. R. Soc. Lond. A* **400,** 97–117 (1985).
3. Cirac, J. I. & Zoller, P. Quantum computations with cold trapped ions. *Phys. Rev. Lett.* **74,** 4091–4094 (1995).
4. Monroe, C., Meekhof, D. M., King, B. E., Itano, W. M. & Wineland, D. J. Demonstration of a fundamental quantum logic gate. *Phys. Rev. Lett.* **75,** 4714–4715 (1995).
5. Cory, D. G., Fahmy, A. F. & Havel, T. F. Ensemble quantum computing by NMR spectroscopy. *Proc. Natl Acad. Sci. USA* **94,** 1634–1639 (1997).
6. Gershenfeld, N. A. & Chuang, I. L. Bulk spin-resonance quantum computation. *Science* **275,** 350–356 (1997).
7. Jones, J. A. & Mosca, M. Implementation of a quantum algorithm to solve Deutsch's problem on a nuclear magnetic resonance quantum computer. *J. Chem. Phys.* (in the press); also LANL preprint quant-ph/9801027.
8. Chuang, I. L., Vandersypen, L. M. K., Zhou, X., Leung, D. W. & Lloyd, S. Experimental realization of a quantum algorithm. *Nature* **393,** 143–146 (1998); also LANL preprint quant-ph/9801037.
9. Grover, L. K. in *Proc. 28th Annual ACM Symp. on Theory of Computation* 212–218 (ACM, New York, 1996).
10. Grover, L. K. Quantum mechanics helps in searching for a needle in a haystack. *Phys. Rev. Lett.* **79,** 325–328 (1997).
11. Boyer, M., Brassard, G., Høyer, P. & Tapp, A. in *Proc. 4th Workshop on Physics and Computation—PhysComp '96* (eds Toffoli, T., Biafore, M. & Leão, J.) 36–41 (New England Complex Systems Institute, Boston, MA, 1996).
12. Chuang, I. L., Gershenfeld, N. & Kubinec, M. Experimental implementation of fast quantum searching. *Phys. Rev. Lett.* **80,** 3408–3411 (1998).
13. Laflamme, R., Knill, E., Zurek, W. H., Catasti, P. & Mariappan, S. V. S. NMR GHZ *Proc. R. Soc. Lond. A* (in the press).

Carbon nanotubule membranes for electrochemical energy storage and production

Guangli Che, Brinda B. Lakshmi, Ellen R. Fisher & Charles R. Martin

Department of Chemistry, Colorado State University, Fort Collins, Colorado 80523, USA

....

Ensembles of aligned and monodisperse tubules of graphitic carbon can be prepared by a templating method[1–4] that involves the chemical-vapour deposition of carbon within the pores of alumina membranes[5–7]. Tubules with diameters as small as 20 nm have been prepared in this way[7,8]. The carbon comprising these tubules can be transformed from a disordered material to very highly ordered graphite[5]. Here we show that template-synthesized carbon tubules can be fabricated as free-standing nanoporous carbon membranes, and that narrower, highly ordered graphitic carbon nanotubes can be prepared within the membrane's tubules. Both the outer and the inner tubules are electrochemically active for intercalation of lithium ions, suggesting possible applications in lithium-ion batteries[9,10]. The membranes can also be filled with nanoparticles of electrocatalytic metals and alloys. Such catalyst-loaded membranes can be used to electrocatalyse O_2 reduction and methanol oxidation, two reactions of importance to fuel-cell technology.

Carbon nanostructures are of tremendous interest[10,11], from both a fundamental and an applied perspective. Applications investigated include use for storage of hydrogen[12] and other gases[13], as a catalyst support[10,11,14,15] and as a tip for scanning probe microscopy[16,17]. In addition, participants at the recent Rice University Workshop on these structures have suggested[11] that these tubes might be used as membrane materials for batteries and fuel cells, anodes for lithium-ion batteries, capacitors, and chemical filters. Many of these proposed applications will require alignment[11,18] of the nanotubules and aggregation of these aligned tubes to form a membrane. We have accomplished these objectives and have used the resulting aligned carbon-tubule membranes to demonstrate some of these proposed energy-related applications.

The previously described chemical-vapour deposition (CVD) method[5] was used to synthesize the carbon tubules within the pores (200-nm-diameter) of a commercially available alumina template membrane[1,5]. (Although this method has been used to make carbon tubules with diameters as small as 20 nm (ref. 7; G.C. and C.R.M., unpublished results), we have found it a good strategy to begin with membranes with larger pore diameters.) This membrane has 60% porosity and is ~60 μm thick. In addition to producing a carbon tubule within each pore, the CVD method yields carbon surface films (~20 nm thick) that cover both faces of the alumina membrane[5]. This is important because these surface films will be used to hold the tubules together, in an aligned fashion, after removal of the underlying alumina membrane (see below).

For all of the energy-related applications described here, catalytic metal nanoparticles were then prepared within the CVD template-synthesized carbon tubules. This was accomplished by immersion of the C/alumina membrane into a solution of the desired metal ion, either 73 mM H_2PtCl_6 (aqueous)[7], 37 mM H_2PtCl_6 plus 73 mM $RuCl_3$ (aqueous), or 124 mM $Fe(NO_3)_3$ (ethanolic)[18]. After immersion, the membrane was dried in air, and the ions were reduced to the corresponding metal or alloy by a 3-h exposure to flowing H_2 gas at 580 °C. The underlying alumina was then dissolved away in 46% HF solution to obtain the desired free-standing carbon-tubule membrane. The alumina dissolution process can be followed visually because the high temperature (900 °C) used in the CVD synthesis[5] causes the alumina to curl into a tight cylinder. As the underlying alumina is dissolved by the HF, this cylinder relaxes, ultimately producing the desired planar, free-standing, carbon-tubule membrane, suspended in the HF solution. This membrane was removed from the HF solution and rinsed with water.

The scanning electron micrograph in Fig. 1a shows that the carbon tubules that make up these membranes are aligned, and that the ends of these tubules are open. Fig. 1b shows a transmission electron micrograph of a single tubule that was removed (by ultrasonification) from such a membrane. The tubule walls are sufficiently thin that the Pt/Ru nanoparticles contained within can be seen. Images of this type were used to obtain the following particle size distributions: Pt (7.1 ± 0.4 nm), Pt/Ru (1.59 ± 0.03 nm). Iron nanoparticles of this type can be used as catalysts for the CVD growth of highly ordered graphitic-carbon nanotubes[5,18]. This approach was used to grow such nanotubes within the template-synthesized tubules. Figure 1c shows that graphitic nanotubes that wind their way through the template-synthesized tubules are obtained.